Heat Transfer, Volume 51, Issue 6, September 2022, pp. 4950-4976
DOI:10.1002/htj.22530

Magneto-convection around an elliptic cylinder placed in a lid-driven square enclosure subjected to internal heat generation or absorption

Olalekan Adebayo Olayemi[**1, 2], Khaled Al-Farhany[*3], Adebowale Martins Obalalu[4], Tomisin Favour Ajide[1], Kehinde Raheef Adebayo[5]

[1]Department of Aeronautics and Astronautics, Faculty of Engineering and Technology, Kwara State University, Malete, Kwara State, Nigeria.

[2]School of Engineering, Cranfield University, Cranfield, United Kingdom.

[3]Department of Mechanical Engineering, University of Al-Qadisiyah, Iraq.

[4]Department of Physics, Augustine University, Ilara-Epe, Lagos State, Nigeria.

[5]Department of Food and Agricultural Engineering, Faculty of Engineering and Technology, Kwara State University, Malete, Kwara State, Nigeria.

[*]Corresponding email: khaled.alfarhany@qu.edu.iq

[**]Corresponding email: olalekan.olayemi@kwasu.edu.ng; olalekan.a.olayemi@cranfied.ac.uk

Abstract

The impacts of MHD and heat generation/absorption on lid-driven convective fluid flow occasioned by a lid-driven square enclosure housing an elliptic cylinder have been investigated numerically. The elliptic cylinder and the horizontal enclosure boundaries were insulated and the left vertical lid-driven wall was experienced at a fixed hot temperature, and the right wall was exposed to a fixed cold temperature. COMSOL Multiphysics 5.6 software was used to resolve the non-dimensional equations governing flow physics. A set of parameters such as Hartmann number ($0 \leq Ha \leq 50$), Reynolds number ($10^2 \leq Re \leq 10^3$), Grashof number ($10^2 \leq Gr \leq 10^5$), heat generation-absorption parameter ($-3 \leq J \leq 3$), and elliptical cylinder aspect ratio ($1.0 \leq AR \leq 3.0$) have been investigated. The current study discovered that for low Reynolds number, the adiabatic cylinder aspect ratio of 2.0 provided the optimum heat transfer enhancement for the model investigated, also, the impact of cylinder size diminishes beyond Gr=10^4. But for high Reynolds (Re=1000), the size of the cylinder with AR=3.0 offered the highest heat transfer augmentation. The clockwise flow circulation reduces because of an increase in aspect ratio, which

hinders the flow circulation. In addition, heat absorption supports heat transfer augmentation while heat generation can suppress heat transfer improvement.

Keywords: Elliptic cylinder, Hartmann number, heat generation, absorption, Magneto-Convection.

Nomenclature

a	Semi-major axis
AR	Aspect ratio
b	Semi-minor axis $[m]$
B_o	Magnetic induction [Tesla]
g	Acceleration due to gravity $[m/s^2]$
Ha	Hartmann number
J	Dimensionless heat generation coefficient
k	Thermal conductivity $[W/mK]$
L	Dimensionless height of the enclosure
Nu	local Nusselt number
$\overline{\text{Nu}}$	Average Nusselt number
p	dimensional pressure [Nm^{-2}]
P	dimensionless pressure
Pr	Prandtl number
Q_o	Heat generation or absorption coefficient
Ra	Rayleigh number
Re	Reynolds number
T	Dimensional temperature [K]
T_c	Dimensional cold wall temperature [K]
T_h	Dimensional hot wall temperature [K]
u, v	Dimensional velocity components [ms^{-1}]
U, V	dimensionless velocity components
x, y	dimensional Cartesian coordinates $[m]$
X, Y	dimensionless Cartesian coordinates

Greek Symbols

α	thermal diffusivity [m^2s^{-1}]
v	kinematic Viscosity [m^2s^{-1}]
σ	Electrical conductivity [Sm^{-1}]
ρ	density [kgm^{-3}]
φ	dimensionless temperature
Ψ	dimensionless stream function

1 Introduction

Mixed convection in enclosures of various configurations has captured numerous researchers' interest over the years owing to its broad technological engagements such as in the cooling of electronic devices, nuclear reactors, chemical processing equipment, lubricating groves, and in the manufacturing of float glass and coating. Some of the previous works done on mixed convective heat transfer are captured in [1-6]. Olayemi et al. [7] considered lid-driven convective flow in a square cavity exposed to different modes of heating and submitted that the maximum heat transfer took place close to the lower wall of the domain considered with the occurrence of the highest value of mid-plane flow velocity at y=0.4. Khan et al. [8] analyzed lid-driven convective flow in a trapezoidal configuration housing a cylinder that was subjected to rotary motion. Reports from the analysis show that for large wall orientation angle when the Grashof number is lowered the heat transfer rate decreases. Yang and Farouk [9] researched mixed convective flow in a circular

domain equipped with a heated rotating square cylinder. The report opined that as the inner-to-outer cylinder ratio increases, *Nu* decreases. Chamkha et al. [10] reported studies on the inner rotary motion that occurred in a porous cavity. According to their findings, the average and local heat transfer coefficients rise when the cylinder approaches either the upper or lower regions of the domain considered.

Olayemi et al. [11] considered buoyancy-dependent flow in a square domain which housed a heated rectangular obstacle; the assessment conducted revealed that at $AR=0.1$, the Nu_{av} is invariant at the orientation of 0° and 90°. Ismael et al. [12] analyzed mixed convective flow in a porous domain containing two spinning cylinders. The study revealed that the local heat transfer coefficient is a direct function of *Ra*. Khajeh et al. [13] considered lid-driven convective heat transfer of Al_2O_3 on elliptical configurations with entropy generation incorporated. They showed that in the presence of irreversibility, heat transfer augmentation was achieved. Saieed et al. [14] numerically investigated an inclined circular enclosure driven by buoyancy in the existence of an elliptic heat source. It was reported that at high *Ra* values, the heat transfer rates improved as the inner cylinder inclination angle increased. The influence of internal heat-generating elliptic block in a porous lid-propelled square domain was examined by Bhuiyan and Munshi [15]. For high values of Darcy and Gasthof numbers, it was observed that streamlines and isotherms were completely dispersed throughout the domain analyzed.

Alam et al. [16] evaluated mixed convective flow in a cavity that was exposed to Joule heating. The study has it that as the *Ra* increases, the local heat transfer coefficient amplifies. Chamkha et al. [17] examined mixed convective flow under the influence of a magnetic field and entropy generation effects of nanofluid in a porous enclosure. The investigation showed that the heat transport strength was found to reduce with magnetic field improvement. The work of Mahfoud et al. [18] looked at the impacts of MHD on the thermal and flow profiles within coaxial cylinders that have been heated from the bottom. Hu [19] used the lattice Boltzmann approach to study the impact of the movement of an elliptical particle in a square enclosure propelled by the lid. It was reported that the vortex location within the enclosure relies on *Re* and that the elliptical particle inertia-imposed circle limits its motion profile. Chamkha [20] considered the convective flow of fluid in a vertical lid-driven enclosure under MHD mode with internal heat production or

absorption. Heat generation/absorption parameters and strength of magnetic field effects on heat transfer enhancement were extensively discussed.

Rahman et al. [21] numerically investigated Joule heating influence on mixed convection in an unenclosed channel under the influence of a magnetic field with the bottom wall heated by a heating element. Their findings revealed that the Joule heating parameter could be utilized to adjust the thermal and flow profiles when the Rayleigh number is high. Mondal et al. [22] evaluated partial wall motion influence in a permeable cavity containing Cu–H_2O nanofluid with a heating element positioned at the center. It was theorized that the heat transfer increased crucially for higher Richardson number and high nanofluid volume fractions. Alam et al. [23] reviewed *Ra* influence on mixed convection in a square geometry having an undulating wall. Rajarathinam et al. [24] investigated the thermal characteristics in an oriented porous cavity containing Cu-H_2O nanofluid. They found that the thermal profile improved with Darcy number and volume fraction of nanofluid. Nosonov and Sheremet [25] in the presence of a local heater considered mixed convective fluid flow in a rectangular domain. It was revealed that growth in Richardson number resulted in forced flow deformation.

El Moutaouakil et al. [26] employed the lattice Boltzmann approach to simulate buoyancy flow around a cylinder of hexagonal cross-section located in a square configuration. It was reported that the number of convective cells formed is governed by the size of the hexagon and Rayleigh number. Soomro et al. [27] explored MHD mixed convection in a triangular domain having a circular barrier. Both the thermal and fluid profiles were found to be a function of wall motion and the barrier situated in the enclosure. Taamneh and Bataineh [28] analyzed the thermal characteristics in a square cavity containing Al_2O_3-H_2O nanofluid and driven by the lid. The study has it that nanoparticle addition to base fluid improved the thermal profile of the flow. Xiong et al. [29] analyzed obstacle location influence on thermal and fluid flow characteristics in a triangular domain; it was opined that Richardson number improvement amplified the rate of transfer of heat. Moreover, Al-Farhany and Abdulsahib [30] in a two-layered nanofluid and saturated porous media considered mixed convective flow in a square domain containing an inner cylinder which is subjected to rotary motion. The study demonstrated that the Nusselt number improved with Rayleigh number improvement. Similar results were reported for a previous study by Abdulsahib and Al-Farhany [31] for high Darcy numbers. Deb et al. [32] numerically analyzed a lid-driven cavity housing an elliptical barrier subjected to Joule heating. Adekeye et al. [33] simulated the

effects of both fluid properties and some selected geometrical parameters on magnetohydrodynamic convective flow in a tilted porous elliptical enclosure exposed o localized heating. It was opined that the flow circulation decreased with growth in Hartmann number. Toghraie and Shirani [34] simulated lid-driven convective flow occurring in a cavity. It was infrenced that Richardson number improvement enhanced heat transfer. Das et al. [35] reviewed the strategies that have been employed by researchers to augment heat transfer in both forced and mixed convective heat transfer scenarios in different geometries. Padhi et al. [36] analyzed mixed convective flow in a cavity with regard to the formation of eddies. It was established that magnetic field strength improvement resulted in the velocity profiles being subdued thus giving rise to recirculation sections. Alomari et al. [37] analyzed MHD impacts on a trapezoidal cavity containing hybrid nanofluid. The trapezium was exposed to sinusoidal heating from below. In the study, Nu_{av} improved directly with both Ra and hybrid volume fraction improvement, but inversely with the Ha. Venkatadri et al. [38] considered mixed convective flow in a square domain having its left vertical wall subjected to central heating.

Based on the literature search conducted, the uniqueness of the current work is that mixed magneto-convection in a square enclosure equipped with internal heat generation or absorption modes and containing an adiabatic elliptic cylinder has not been considered previously. This investigation contributes to heat transfer augmentation without accruing extra energy and materials particularly for low Re flow regimes. Additionally, the heat transfer profile of the current investigation underpins the import of dimensionless numbers such as Hartmann number, adiabatic barrier aspect ratio, heat generation/absorption parameter on the mechanism of transport of laminar combined convection in shear and buoyancy-driven enclosure. The current study finds practical signifance in microelectronic devices, solar and nuclear reactor technologies, geothermal energy systems among others.

2 Methodology

2.1 Description of the Physical Model

Figure 1 illustrates a two-dimensional representation of the physical model employed for the current investigation. The model consists of an elliptic cylinder centered in a square enclosure with an aspect ratio of ($AR = \frac{a}{b}$); where a is the length of the major axis and b is the minor axis of the

ellipse. The space created by the elliptic cylinder and the enclosure is filled with a heat-conducting or absorbing fluid subjected to magnetic influence. The enclosure's flow is taken to be laminar and driven by a mixed convective mechanism. The walls of the elliptic cylinder and the horizontal boundaries of the domain are insulated.The left and right boundaries of the model are sustained at fixed thermal values of T_h and T_c respectively. The density changes were accounted for by the Boussinesq model, and fluid properties are assumed constant. No-slip velocity was imposed on all the walls except the left vertical wall, which was assumed a lid-driven wall.

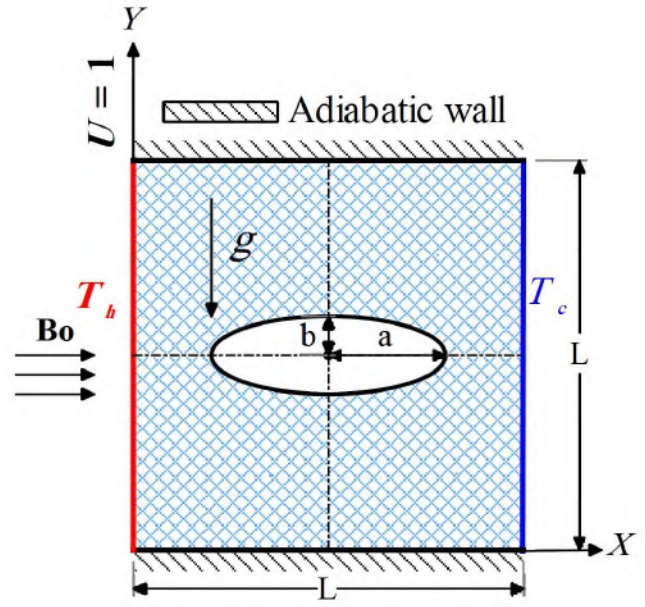

Figure 1: Geometry

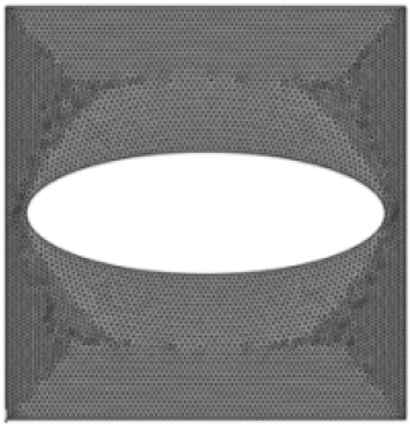

Figure 2: Mesh Distribution

2.2 Governing equations

The equations of interest in dimensionless forms are as follows:

Continuity [16, 21]:

$$\frac{\partial U}{\partial X}+\frac{\partial V}{\partial Y}=0 \tag{1}$$

Momentum transport equations:

X-direction:

$$U\frac{\partial U}{\partial X}+V\frac{\partial U}{\partial Y}=-\frac{\partial P}{\partial X}+\frac{1}{Re}\left[\frac{\partial^2 U}{\partial X^2}+\frac{\partial^2 U}{\partial Y^2}\right] \tag{2}$$

Y-direction:

$$U\frac{\partial V}{\partial X}+V\frac{\partial V}{\partial Y}=-\frac{\partial P}{\partial Y}+\frac{1}{Re}\left[\frac{\partial^2 V}{\partial X^2}+\frac{\partial^2 V}{\partial Y^2}\right]+\frac{Ra}{Re^2 Pr}\varphi-\frac{Ha^2}{Re}V \quad (3)$$

Energy transport equation:

$$U\frac{\partial \varphi}{\partial X}+V\frac{\partial \varphi}{\partial Y}=\frac{1}{RePr}\left(\frac{\partial^2 \varphi}{\partial X^2}+\frac{\partial^2 \varphi}{\partial Y^2}\right)+\frac{J}{Re\,Pr} \quad (4)$$

Transformation parameters

$$X=\frac{x}{L},\ Y=\frac{y}{L},U=\frac{u}{U_o},V=\frac{v}{U_o},\ \varphi=\frac{T-T_c}{T_h-T_c},\ P=\frac{p}{\rho u_o^2},\ Pr=\frac{\upsilon}{\alpha}$$

$$J=\frac{Q_o L^2}{\alpha\rho c_p},Ra=\frac{\rho g\beta(T_h-T_c)L^3}{\mu\alpha},Re=\frac{U_o L}{\upsilon},Ha=B_o L\sqrt{\frac{\sigma}{\rho\upsilon}} \quad (5)$$

2.3 Modeling Procedure

COMSOL 5.6 Multiphysics software was employed for the current investigation. The heat transfer and fluid flow settings in COMSOL Multiphysics were employed to simulate the problem. The generation was achieved by employing the free quadrilateral mesh using different parameters such as AR, Ha, J, Re, and Gr. The meshed computational domain was approximated with the P_1+P_2 interpolation function while the temperature field was discretized by Galerkin's method. To circumvent the requirement of having to stabilize the convective term in momentum equations, the meshes used were finely resolved. Local numerical instabilities were resolved by adding artificial diffusion via the Streamline Upwind Petrov Galerkin's method and the segregated parametric solver was used for the thermal and flow characteristics variables. Biconjugate gradient stabilized iterative method solver was employed for the thermal and fluid flow modules of the commercial software used, Selimefendigil et al. [39].

3. Nusselt number evaluation

The heat transfer along the solid vertical boundaries is calculated by following Radhi [40]; hence, the local and mean Nusselt numbers are expressed respectively by:

$$Nu_L=-k\frac{\partial \varphi}{\partial X} \quad (6) \qquad \overline{Nu}=\frac{1}{L}\int_0^L Nu_L\,dY \quad (7)$$

4. Stream function

The flow motion of the fluid within the annulus of the geometry analyzed is delineated using stream function (Ψ) and it is defined from the velocity components U and V as follows: [41, 42]

$$U = \frac{\partial \Psi}{\partial Y}, \qquad V = -\frac{\partial \Psi}{\partial X} \tag{8}$$

While the stream function equation is defined by equation (9):

$$\frac{\partial^2 \Psi}{\partial X^2} + \frac{\partial^2 \Psi}{\partial Y^2} = \frac{\partial U}{\partial Y} - \frac{\partial V}{\partial X} \tag{9}$$

5. Validation

The integrity of the mesh quality selected was verified by carrying out grid independence examinations for various mesh sizes on $\overline{Nu}$ of the vertical lid-driven wall as displayed in Table 1. As a trade-off between the costs of computing, numerical stability, and enhanced field resolution, extra fine mesh size was adopted for all the numerical experiments performed in this investigation as shown in Figure 2. Additionally, the code used for the present study was inspected by comparing the results of the $\overline{Nu}$ gotten from the analysis of a differentially heated square enclosure whose vertical walls were subjected to insulation in the absence of the adiabatic cylinder with previous works under the same thermal boundary conditions. The results are delineated in Table 2 and it aligns with those of [43-45]. Furthermore, the response of isotherms from the current investigation to heat generation/absorption parameters are compared with those of Chamkha [20] in Figure 3 and the isotherms show good congruence.

Table 1: Grid independence test of $\overline{Nu}$ on the heated vertical lid-driven wall for Gr=10^2, Re=1000, AR=3, J=0, and Ha=0.

Size of Mesh	**Mesh ethe lements**	**Mean Nusselt number**	**% Absolute deviation from mean value of $\overline{Nu}$**
Coarse	3228	8.15	1.092
Normal	4262	8.16	0.971
Fine	5094	8.19	0.607
Finer	6592	8.18	0.728
Extra fine	17278	8.22	0.243
Extremely fine	61046	8.54	3.640

Table 2: Comparison of the $\overline{Nu}$ on the top wall of the cavity for $Pr = 0.71$ and $Gr = 10^2$ with those in literature.

	Nu		
Re	**100**	**400**	**1000**
Khanafer and Chamkha [43]	1.94	3.84	6.33
Iwatsu et al. [44]	2.01	3.91	6.33
Ali et al. [45]	1.93	3.91	6.31
Present work	2.03	3.99	6.21

	Chamkha et al. [20]	Present work
J=3	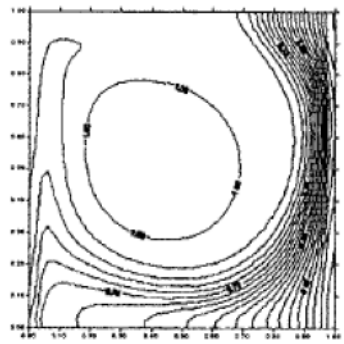	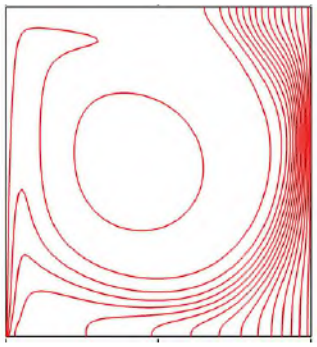
J=1	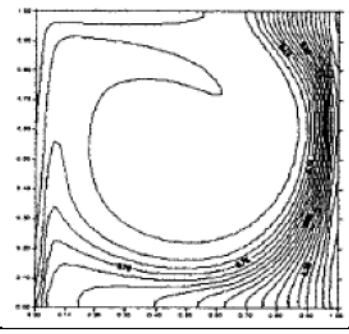	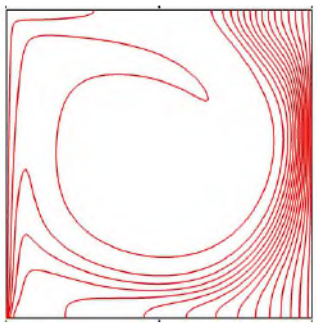
J=-1	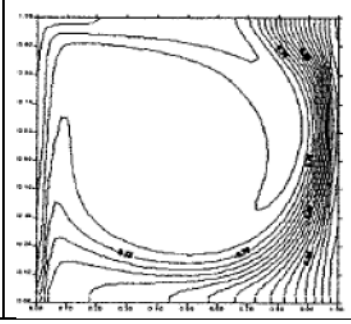	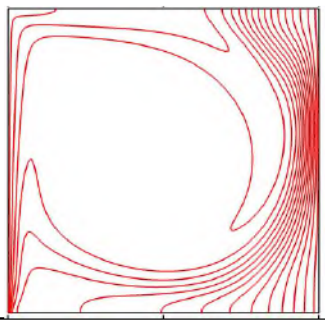

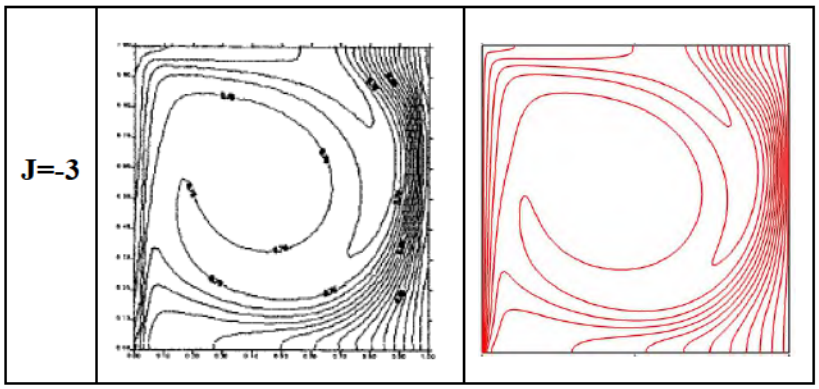

Figure 3: Comparison between the current study (right) with Chamkha et al. [20] study (left) in terms of the effect of the heat generation/absorption on isotherms.

6. Results and discussion

Under this section, the findings for mixed convective heat transfer of a fluid (*Pr=0.71*) that is capable of generating/absorbing heat in the presence of an adiabatic elliptic obstacle positioned in a square domain under the existence of a magnetic field are presented

6.1 Effects of *J, AR,* and *Ha* on Isotherm and stream function

Figures 4-8 display the isothermal plots for the present study where J varies from -3 to +3, Ha from 0 to 50 and AR from 1.0 to 3.0 while Gr=100 and Re=1000. The lines of isotherm near the cavity right wall are closely crowded for all cases, indicating that the temperature gradient around the right wall of the enclosure is steep. In regions that are away from the right wall of the enclosure, the gradient of temperature there is thin because the contour lines are farther apart, this occurrence of the steep gradient is due to the boisterous influence of the shear-driven circulations. The magnetic field influence is such that it inhibits the convective heat transfer mechanism as the isotheral lines are observed to become increasingly parallel to the wall driven by the lid; the heat transport mode in this region is largely due to conduction. When $J=0$, the highest temperature was observed to be on the left wall but as the internal heat generation surges ($J > 0$), the boundary layer assumes more prominence along the vertical boundaries of the enclosure with the maximum temperature drifting from the heated left wall to the isothermal contour lines immediately ahead of the diabatic cylinder; this observation is because the hot fluid that gets to the top insulated wall and those immediately around the adiabatic cylinder are not able to reject heat. However, for the heat absorption ($J < 0$) scenario, the maximum temperatures are observed to be very close to the

hot left wall thereby allowing for a higher heat transport rate. Also, as the magnetic influence (Ha) improves, the adjacent fluid temperatures in the enclosure around the vertical walls approximate the temperature of the respective walls that they are close to thereby reducing the extent of heat transfer enhancement. Finally, as the AR of the adiabatic cylinder increases, the convective force influence improved as seen in the pattern of distribution of the isothermal lines, as a consequence of this, the rate of heat transfer is enhanced.

Figures 9-13 summarize the effects of varying values of *J, H,* and AR on the stream function plots for Gr=100 and Re=1000. For all the stream function plots, the lid-driven hot left wall resulted in the clockwise rotation of main cells and anticlockwise rotation of small corner cells. Because the left moving wall is hot, the shear force and buoyancy force enhance the activity of the recirculation cells. Furthermore, for each of the aspect ratios considered, the effect of a fixed value of applied magnetic force (Ha) for various J values on the stream function is negligible, this shows that Q_o has no major conseque on the secondary flow profile. However, as Ha (strength of magnetic field) increases for a fixed value of J, the strengths of both the primary and secondairy circulations decrease, this is because the Lorentz force (which is produced by the interplay of the electrically conducting flowing fluid and the magnetic field) acts as a current inhibitor. Additionally, when $Ha = 50$ for $AR \leq 2.0$, the secondary circulation around the upper right corner of the square cavity vanishes as a result of further reduction in flow velocity because of the resistance offered by the magnetic force to flow. At Ha =0 and 10, for $2.0 \leq AR \leq 3.0$, there is the formation of a minor cell within the main cell on the lower portion of the ellipse which rotates in a clockwise fashion, but these soon disappear for $Ha > 10$; this observation could be due to the fact that increase in Ha and AR impede flow velocity.

6.2. Influence of aspect ratio (AR) on $\overline{Nu}$

Figures 14 a and b delineate the plots of $\overline{Nu}$ on the hot wall against Grashof number for various aspect ratios of the adiabatic cylinder in the absence of magnetic force ($Ha=0$), heat sink, and heat source ($J=0$). For all the plots, the $\overline{Nu}$ of the hot wall improves with the growth of Grashof number. For Figure 14a, the highest heat transfer augmentation occurred when the adiabatic cylinder axis ratio is 2.0 while the least heat transfer occurred at an axis ratio of 3.0. The observed trend could be because at Re=100, for the range of Grashof numbers considered, convection predominates,

and additionally, the temperature difference between the hot wall at AR=3.0 and the adjoining fluid becomes marginal; hence the heat that would be transferred under this condition should reduce. However, in Figure 14b, heat transfer augmentation improves with the growth of adiabatic cylinder aspect ratio; this is so because force convection predominates and therefore the effect of shear force on the hot wall was able to significantly impose a wide temperature gradient between the hot wall and the adjacent fluid.

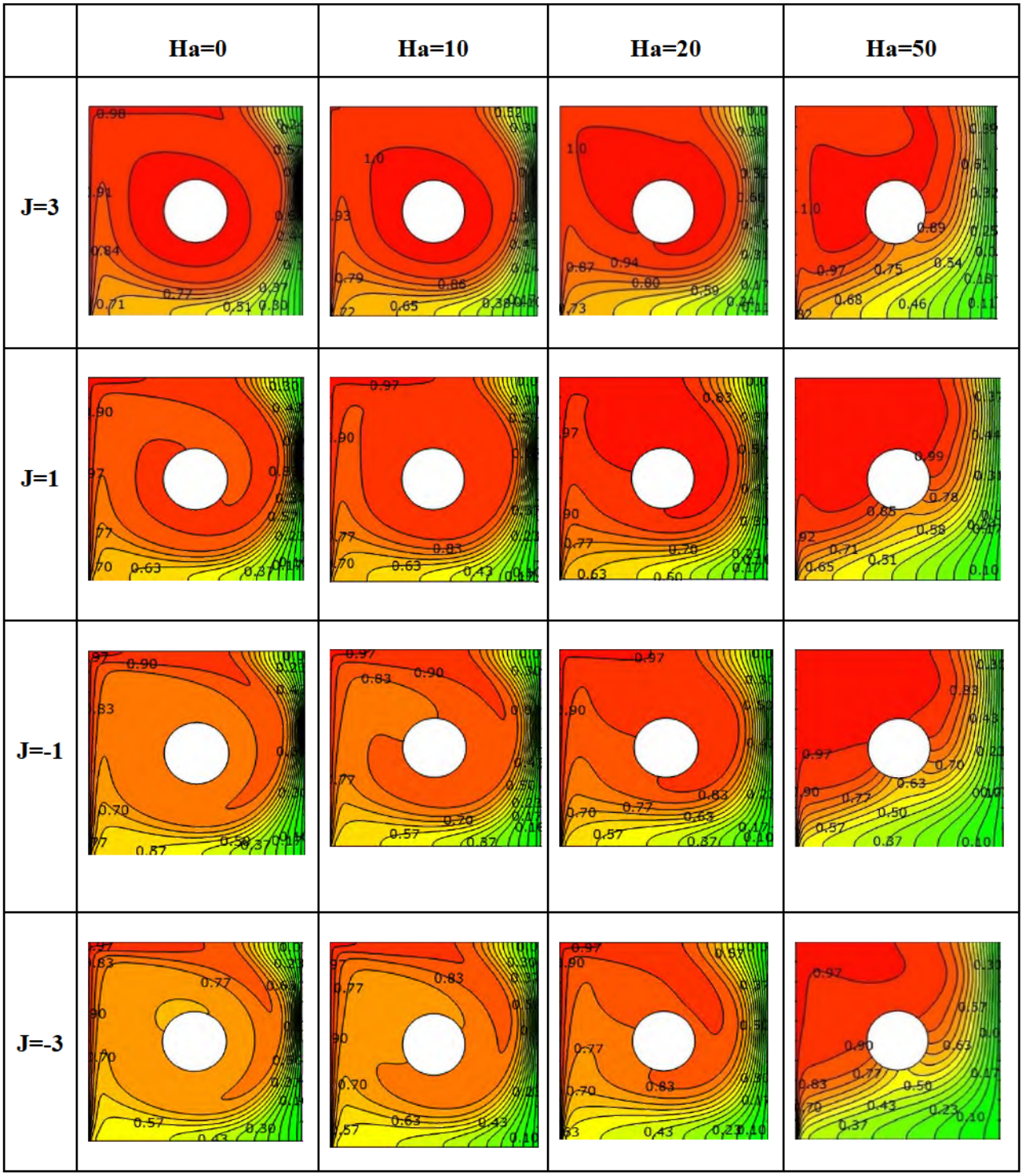

Figure 4: Effects of J and Ha on isothermal contours for Gr=100, Re=1000 and AR=1.0

	Ha=0	Ha=10	Ha=20	Ha=50
J=3	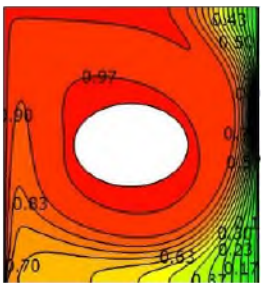	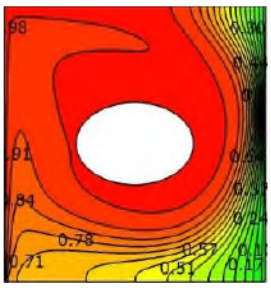	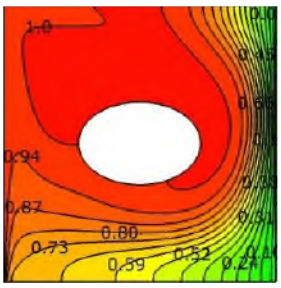	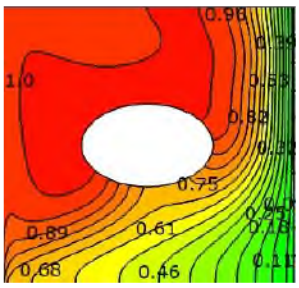
J=1	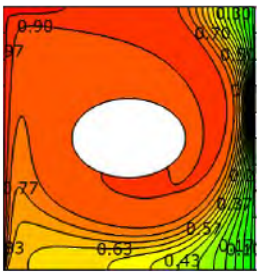	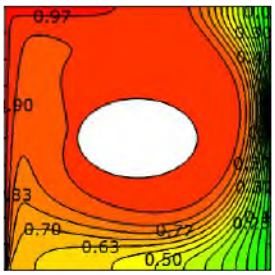	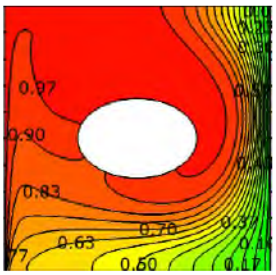	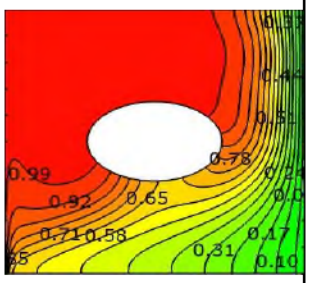
J=-1	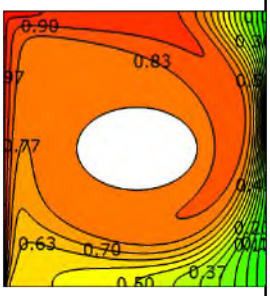	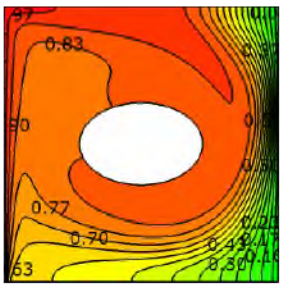	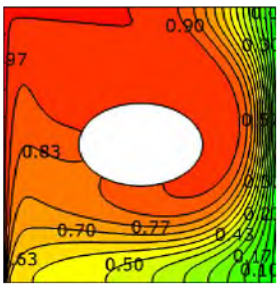	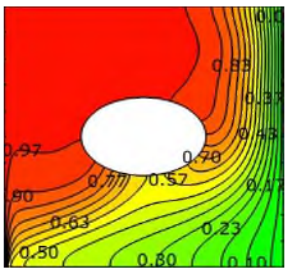
J=-3	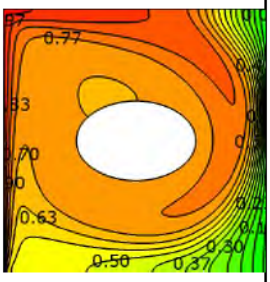	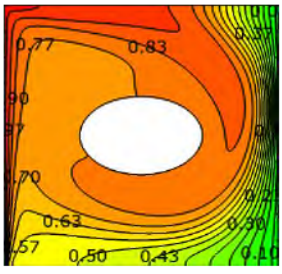	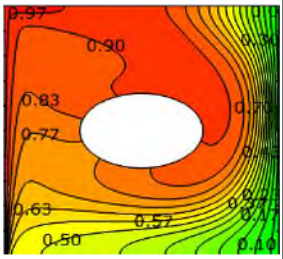	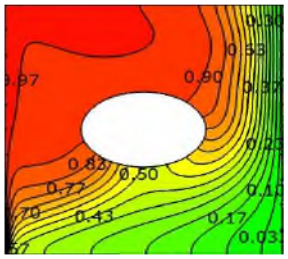

Figure 5: Effects of *J* and *Ha* on isothermal contours for *Gr*=100, *Re*=1000, and *AR*=1.5

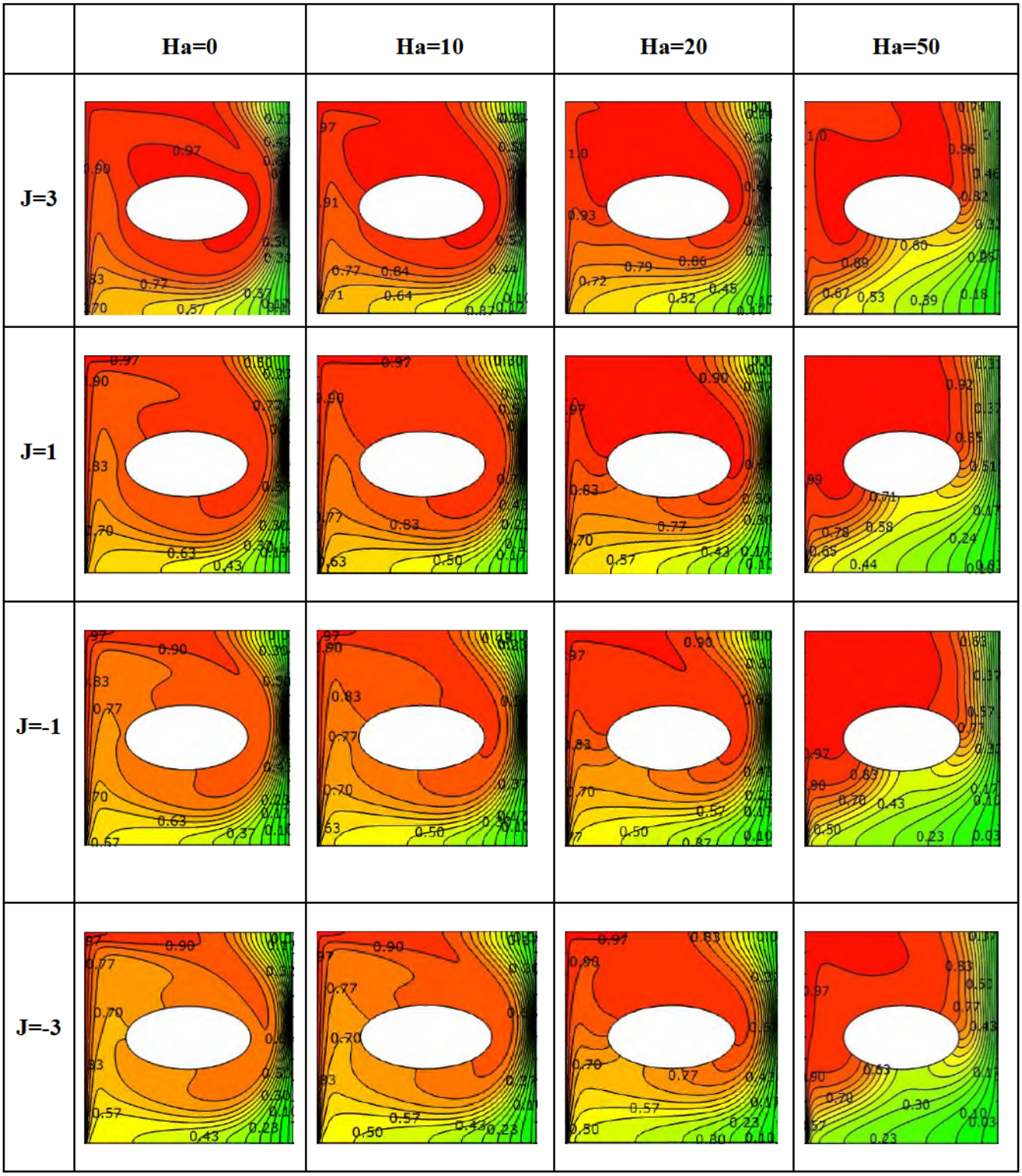

Figure 6: Effects of *J* and *Ha* on isothermal contours for *Gr*=100, *Re*=1000 and *AR*=2.0

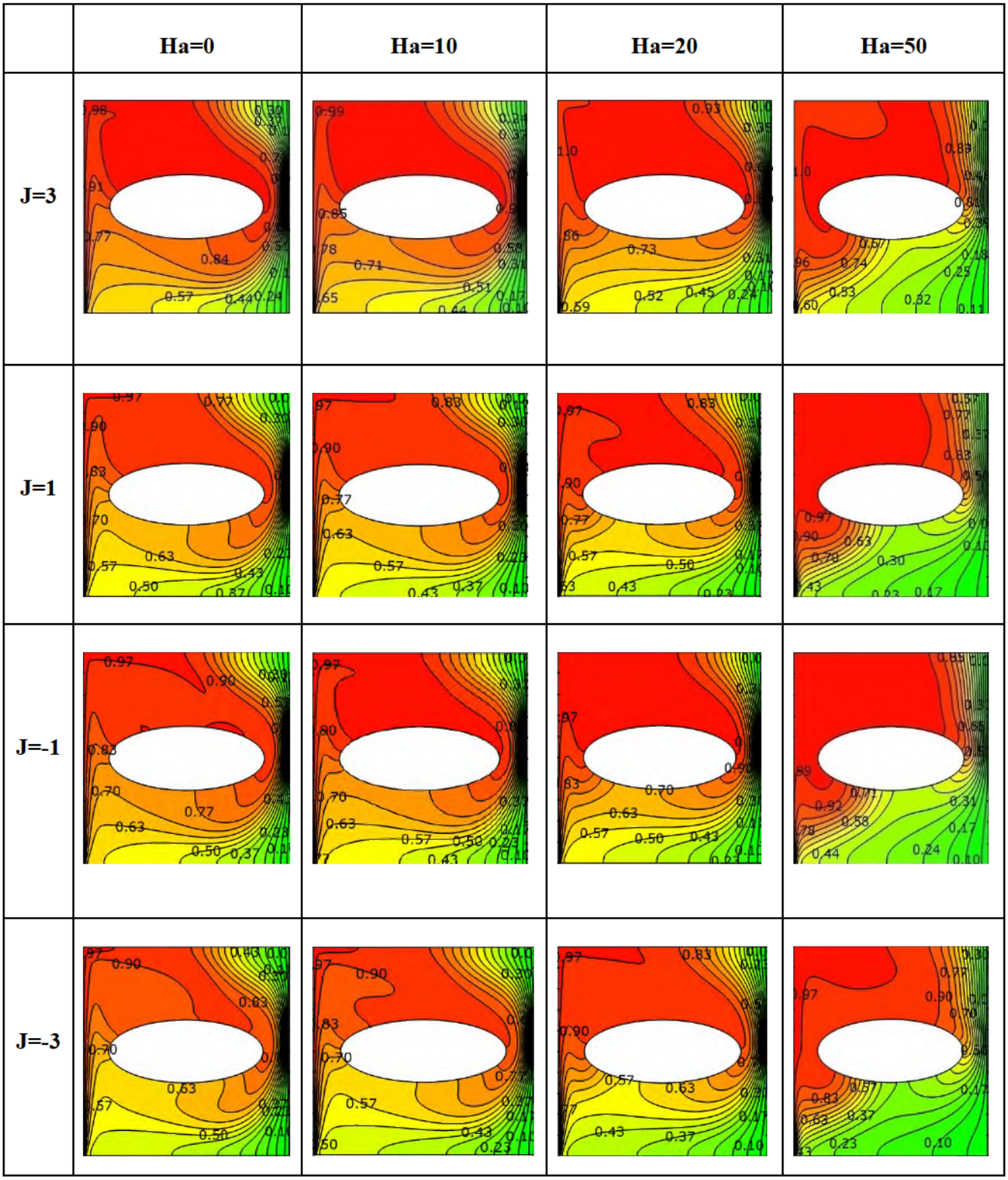

Figure 7: Effects of *J* and *Ha* on isothermal contours for *Gr*=100, *Re*=1000, and *AR*=2.5

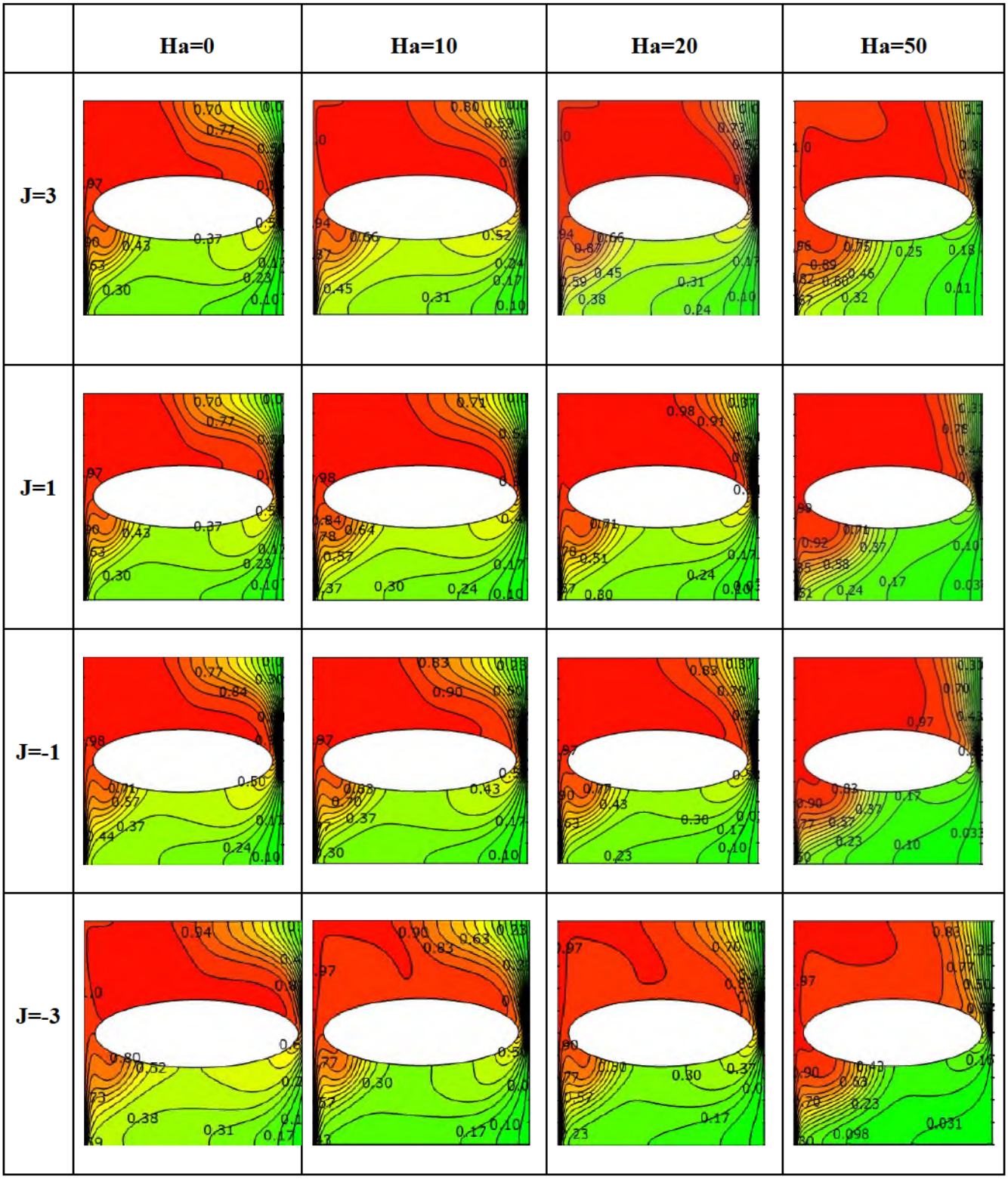

Figure 8: Effects of *J* and *Ha* on isothermal contours for *Gr*=100, *Re*=1000 and *AR*=3.0

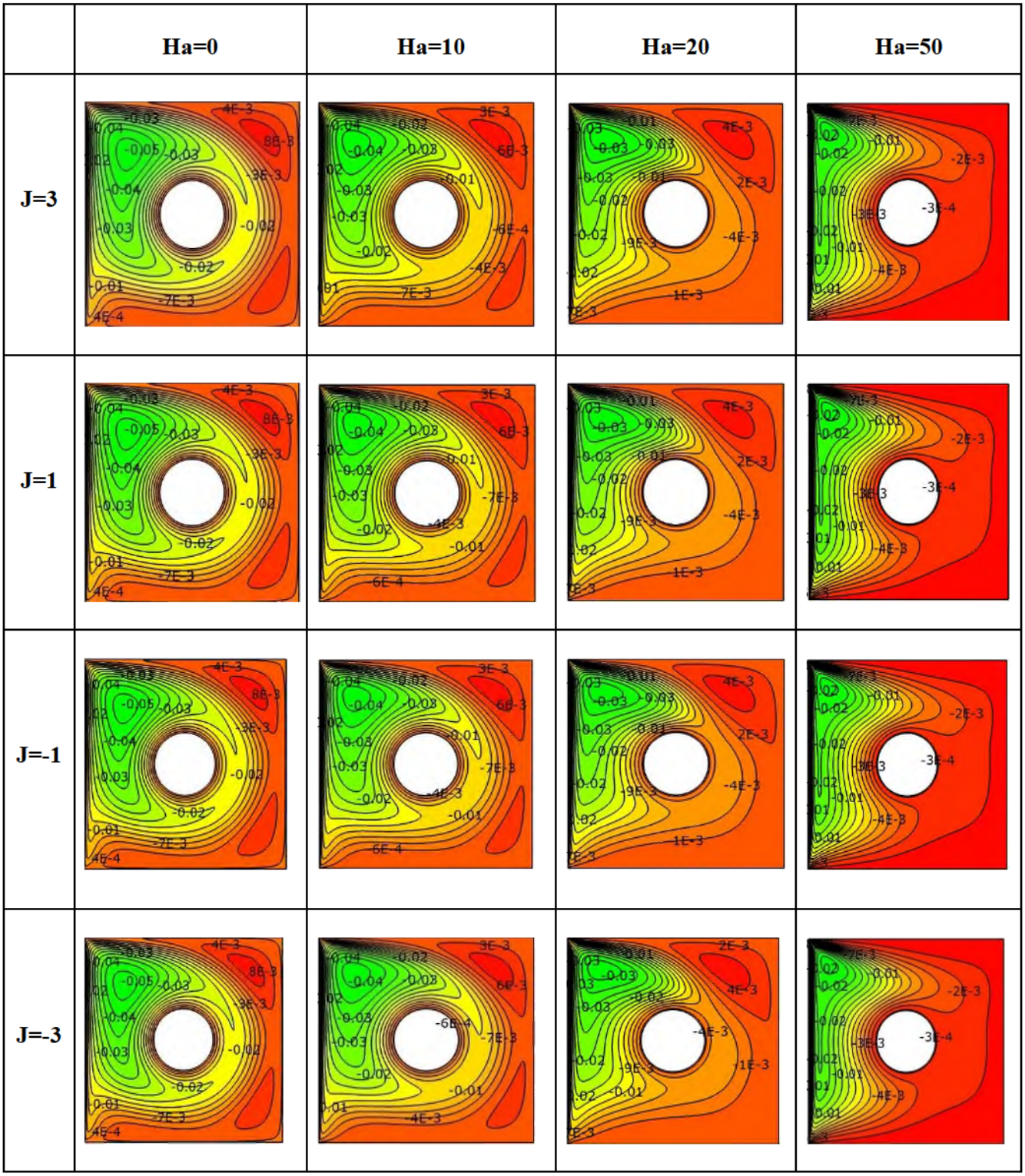

Figure 9: Influence of J and Ha on stream function contours for Gr=100, Re=1000, and AR=1.0

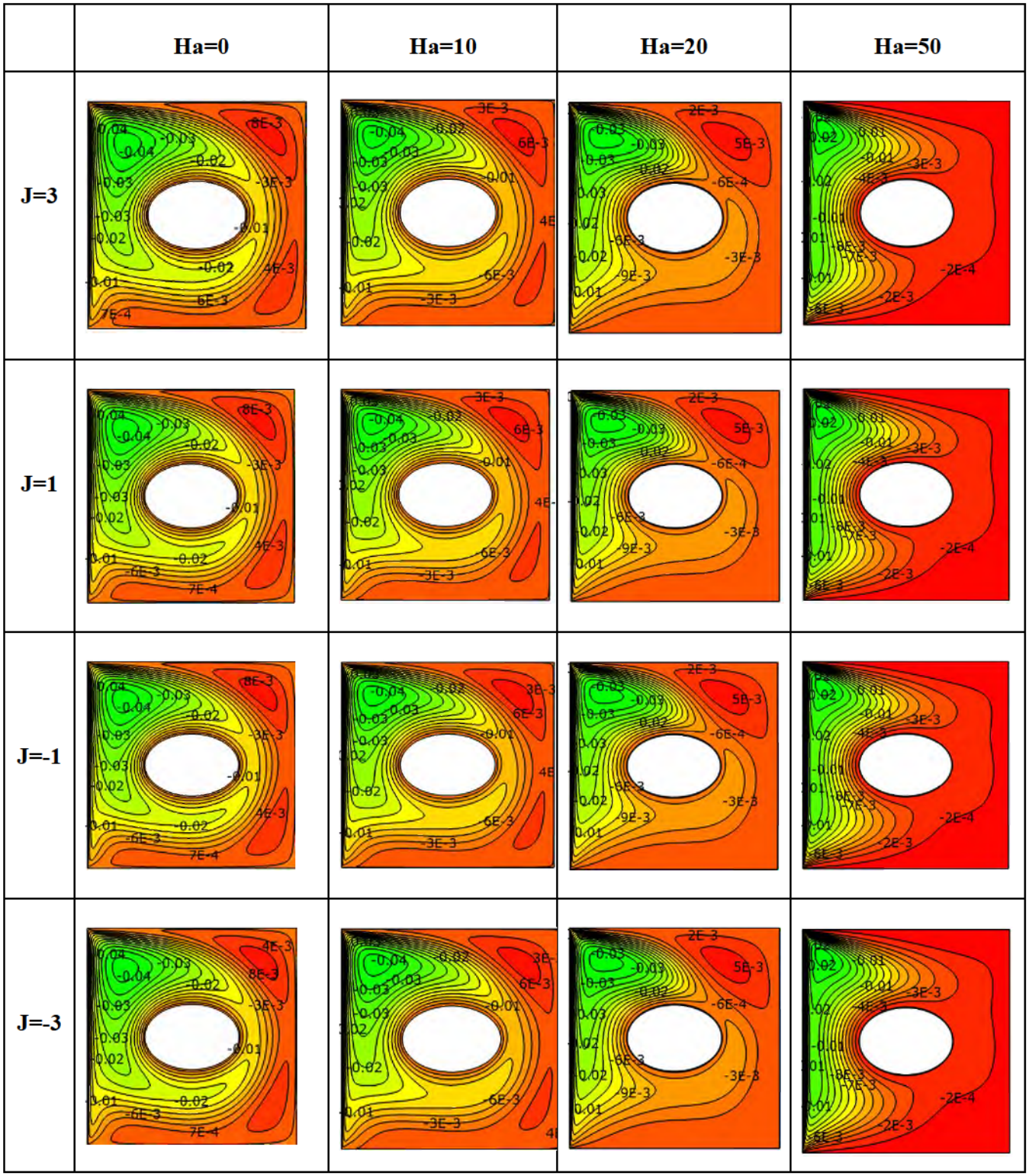

Figure 10: Influence of *J* and *Ha* on stream function contours for *Gr*=100, *Re*=1000, and *AR*=1.5

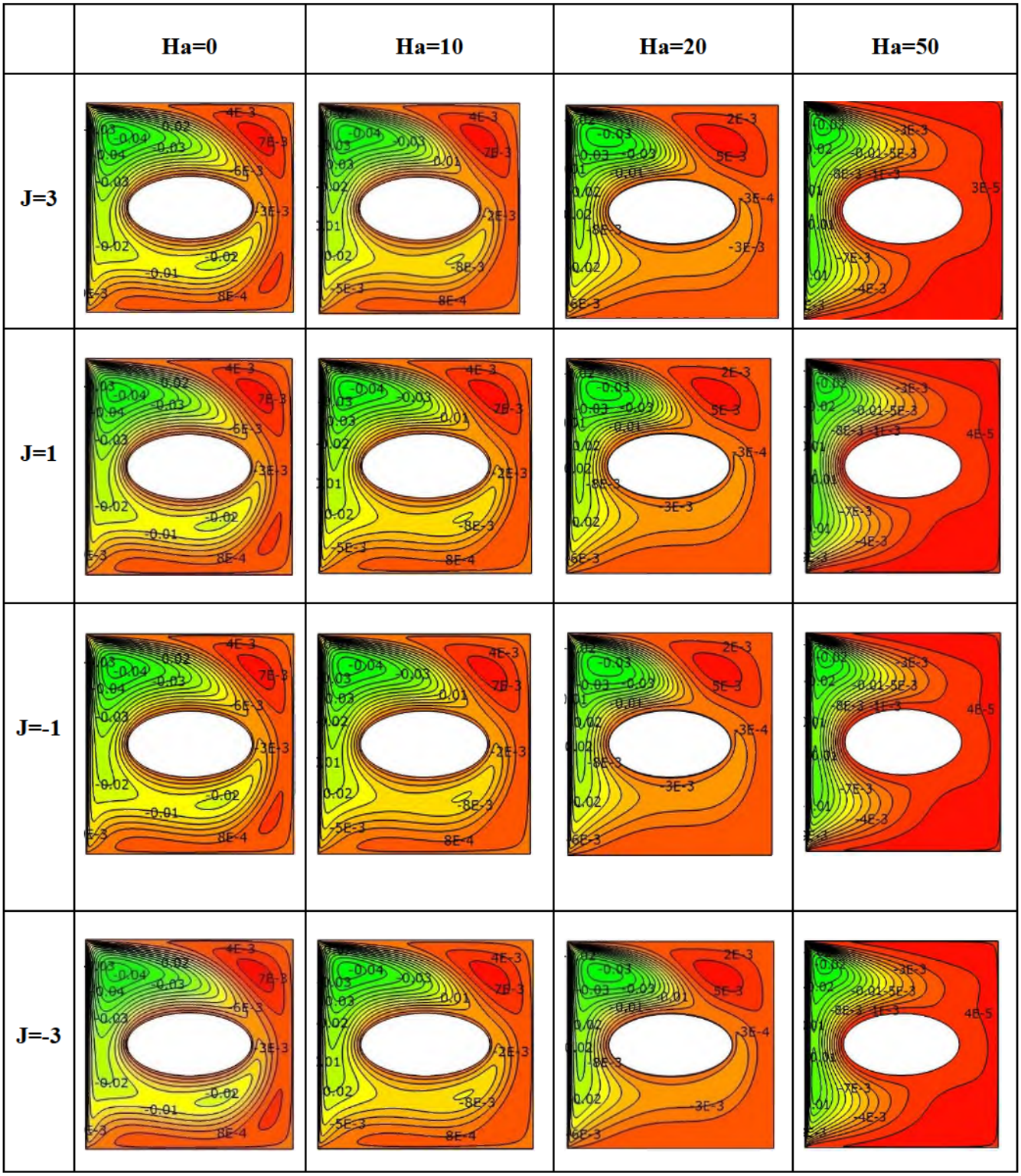

Figure 11: Influence of *J* and *Ha* on stream function contours for *Gr*=100, *Re*=1000, and *AR*=2.0

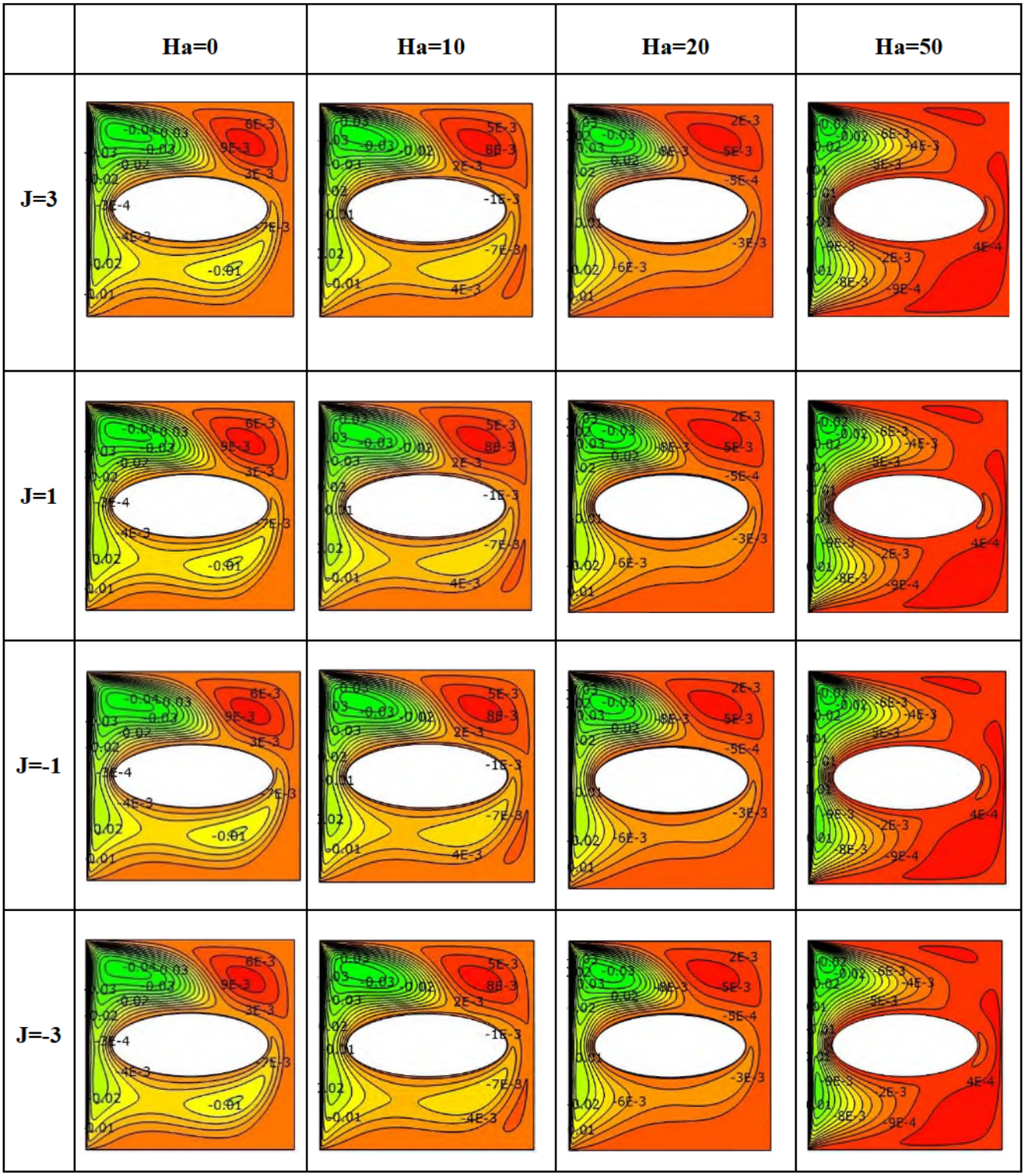

Figure 12: Effects of J and Ha on stream function contours for Gr=100, Re=1000, and AR=2.5

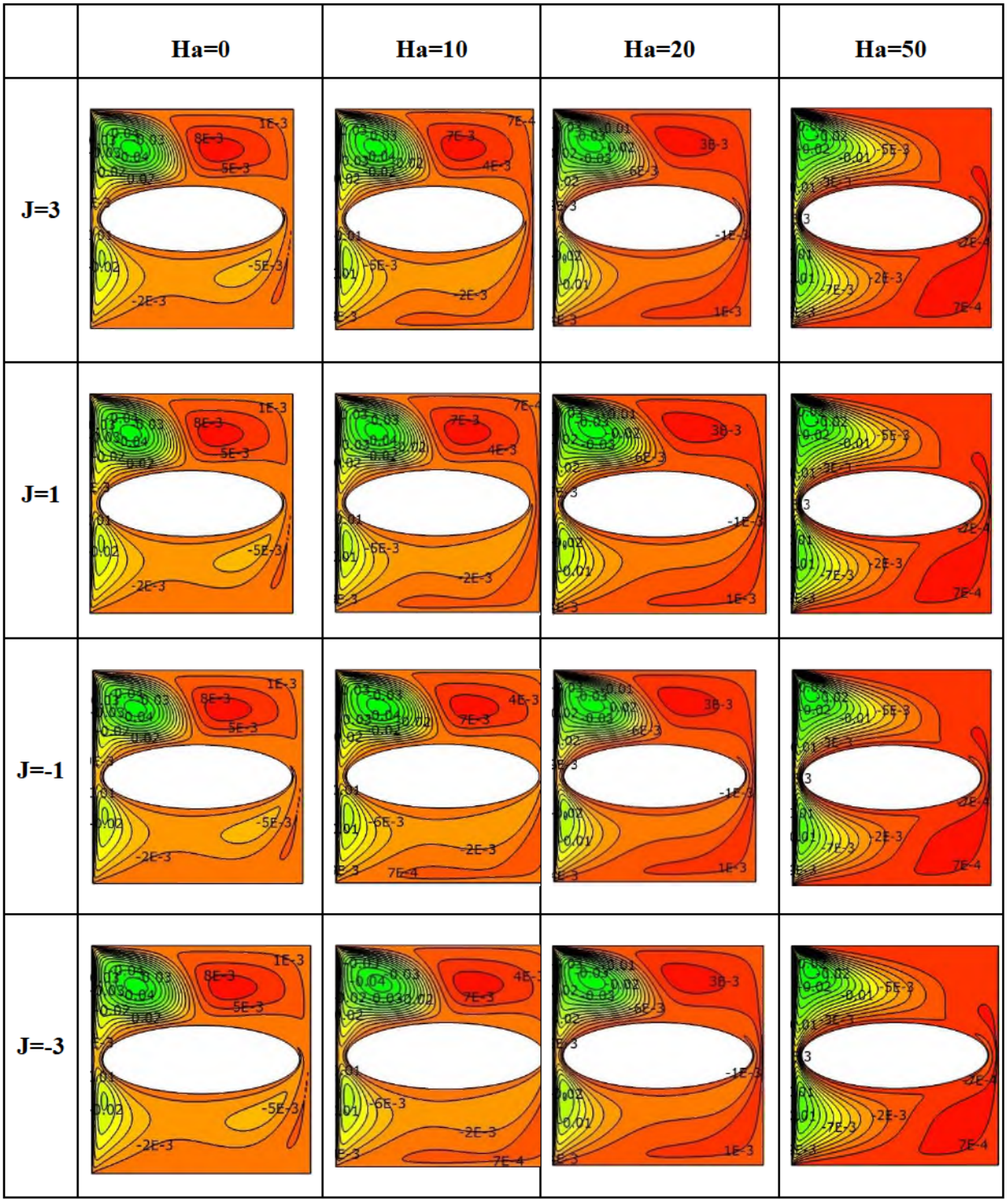

Figure 13: Impacts of J and Ha on stream function contours for Gr=100, Re=1000 and AR=3.0

Generally speaking, when $Ha=J=0$, that is, in the absence of magnetic field and heat-generating or absorbing influence, Richardson number ($Ri=Gr/Re^2$) dictates the relative relevance of buoyancy force as compared to shear force.

6.3. Effect of magnetic force (Ha) on $\overline{Nu}$

The impact of the magnetic force on heat transfer profile for various cylinder aspect ratios in the absence of Q_o is displayed in Figures 15 and 16. All the plots in Figures 15 and 16 reveal that Lorenz force inhibits heat transfer this is due to the fact that Lorentz force acts as a current inhibitor; also at the aspect ratio of AR=3.0, Hartmann number increment from 0 to 10 resulted in a marginal decrease in heat transfer compared to other range of Hartmann numbers considered. Furthermore, higher heat transfer rates were observed in Figure 16 because of the increase in Re from 100 to 1000. This occurrence is because the increase in Re from 100 to 1000 improved the shear force of the wall driven by the lid over the effect of buoyancy force.

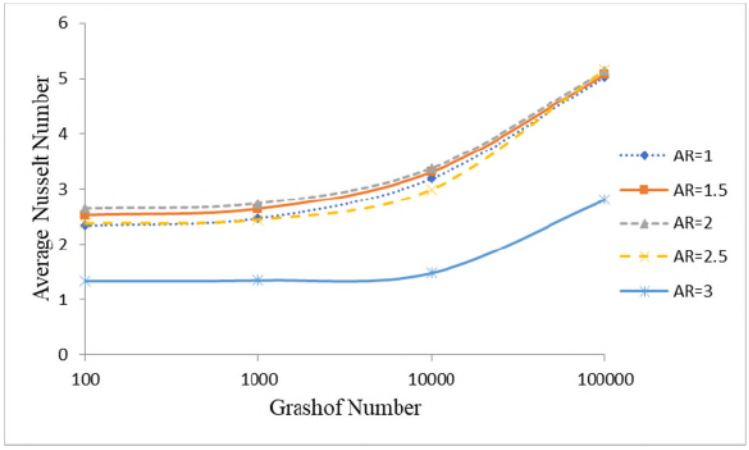

(a)

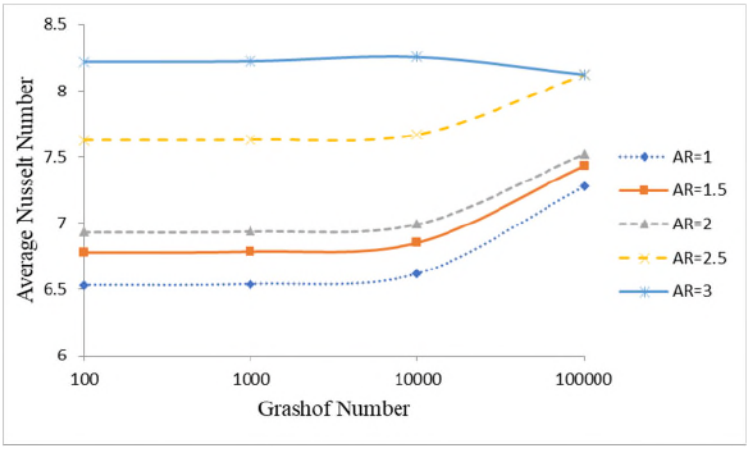

(b)

Figures 14 (a - b): Impact of aspect ratio on Nu*av* for (a) *Re*=100, and (b) *Re*=1000 when *Ha*=*J*=0.

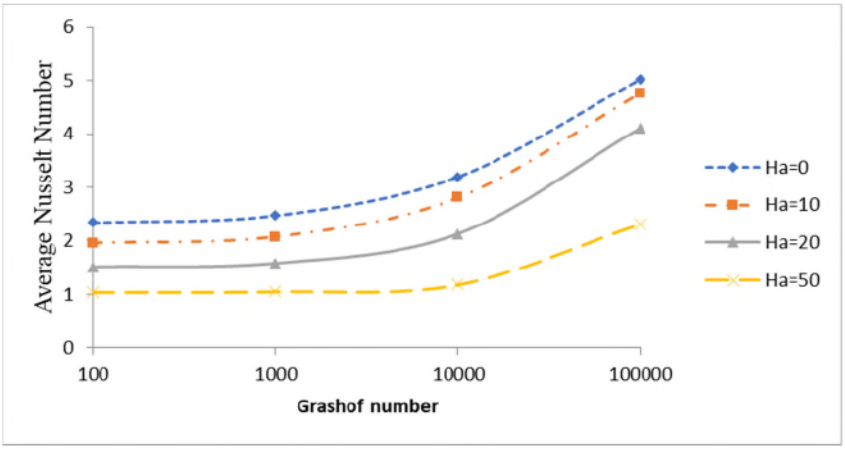

(a)

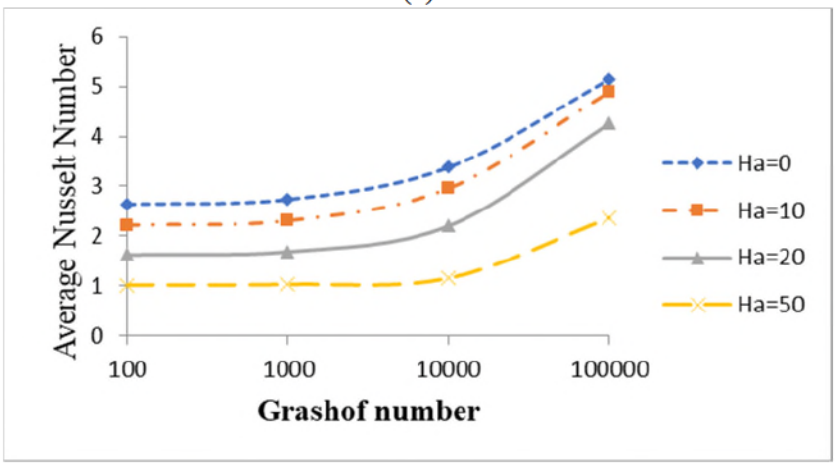

(b)

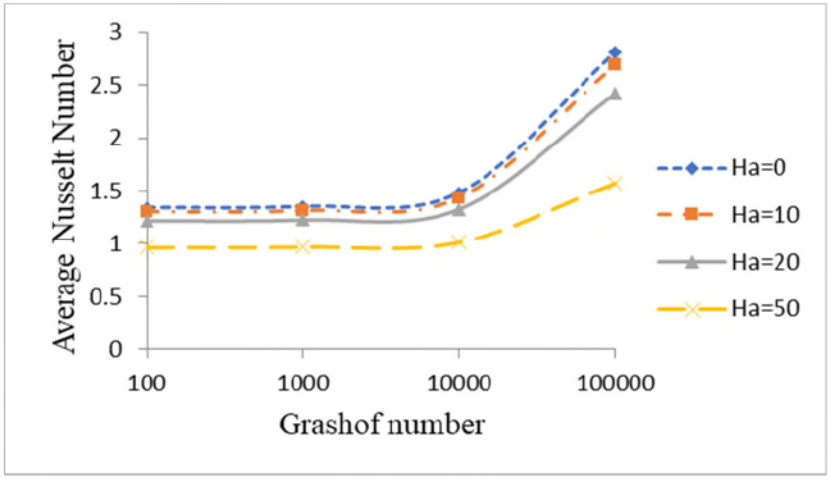

(c)

Figures 15 (a-c): Impact of the magnetic force on Nu_{av} for Re=100, When AR=1.0, 2.0, and 3.0.

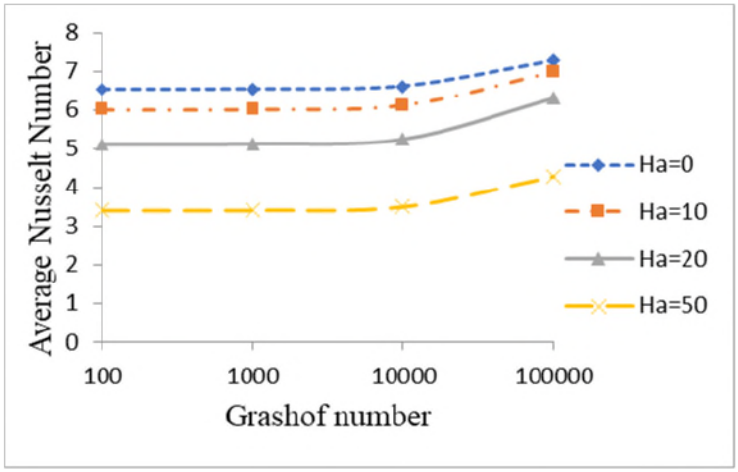

(a)

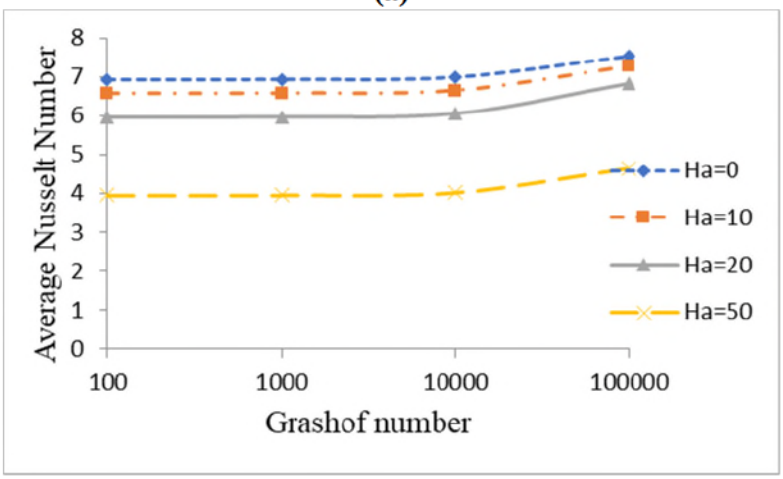

(b)

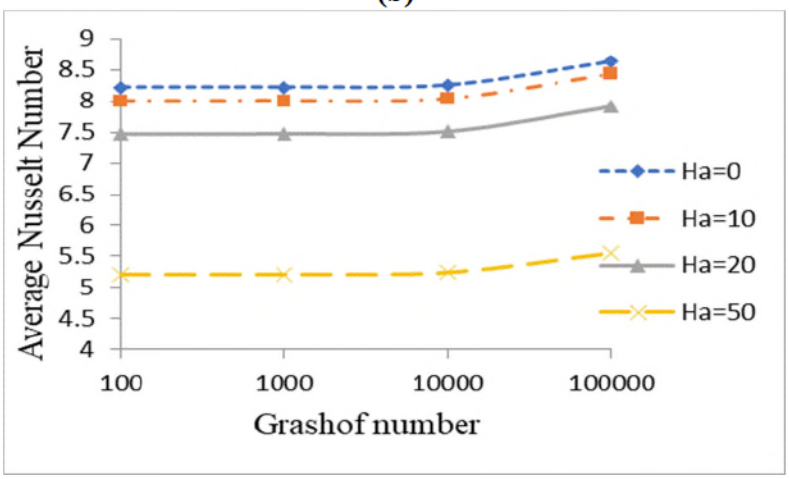

(c)

Figures 16 (a-c): Influence of the magnetic force on *Nuav* for *Re*=1000, when *AR*=1.0, 2.0, and 3.0

6.4. Influence of Internal heat Generation or Absorption (J) on $\overline{Nu}$

The influence of J on the strength of heat transfer is presented in Figures 17 and 18 for different aspect ratios and Reynolds numbers. The plots show that heat augmentation is favored by heat absorption and discouraged by heat generation which is in line with the information provided by the isothermal and stream function plots above that in the vicinity of the left moving wall for the case of heat generation, the temperatures around the lid-driven wall get reduced and the fluid that gets close to the adiabatic top wall get rejected while the converse is true for heat absorption. Furthermore, the influence of aspect ratio and Reynolds number variation as observed in both Figures 17 and 18 are in tandem with the information provided by Figures 14 (a) and (b) which shows that heat transfer enhancement grows with both aspect ratio and Reynolds number improvements. Also, improvement in heat transfer in Figure 17 as compared to Figure 16 for fixed values of Grashof number ($Gr=10^2$-10^6) as Re rises from 100 to 1000 is consistent with what is expected; this observation aligns with the report of Chamka et al. [14].

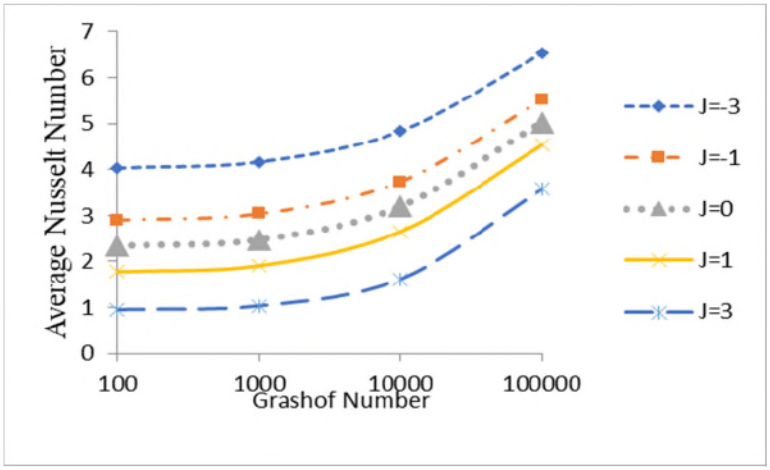

(a)

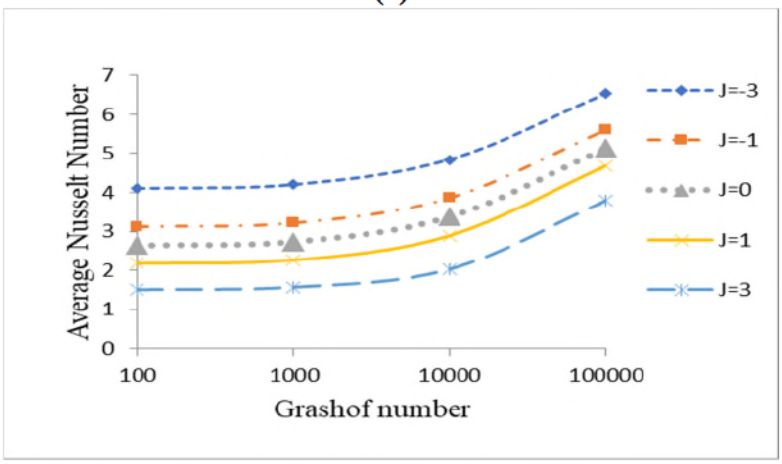

(b)

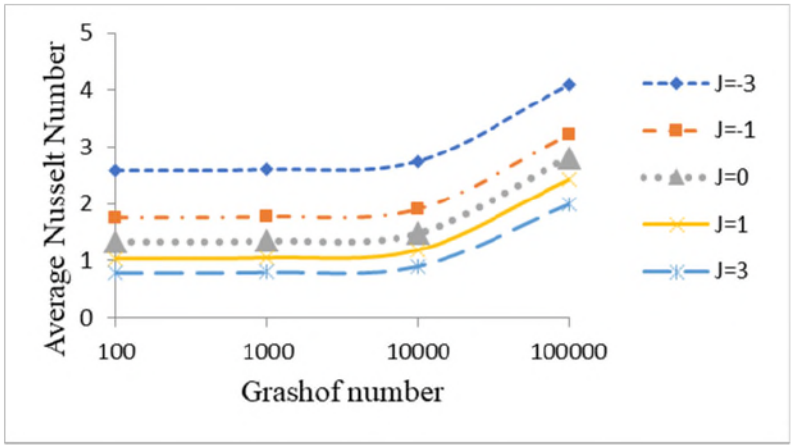

(c)

Figures 17 (a-c): Influence of *J* on Average Nusselt number for *Re*=100, when *AR*= 1, 2, 3.

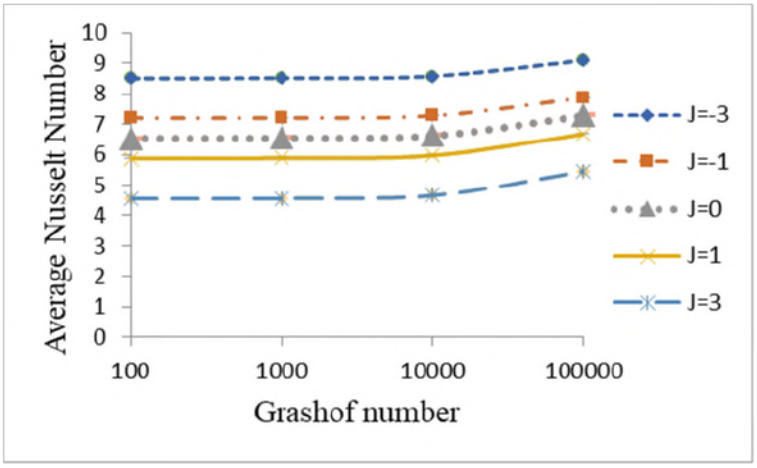

(a)

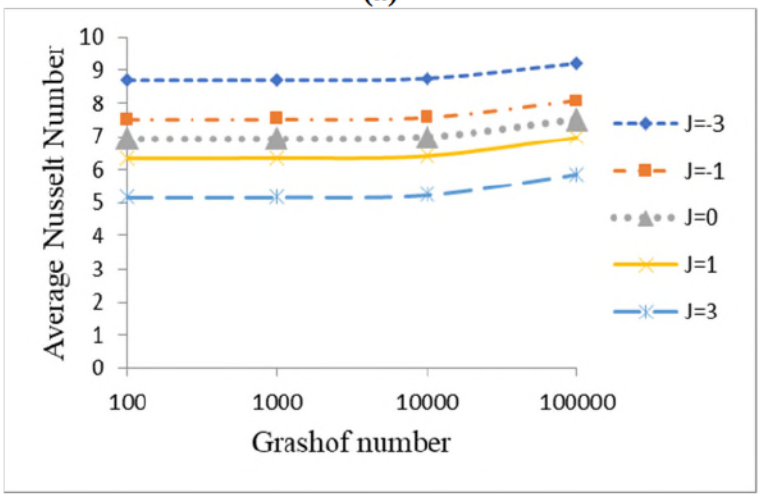

(b)

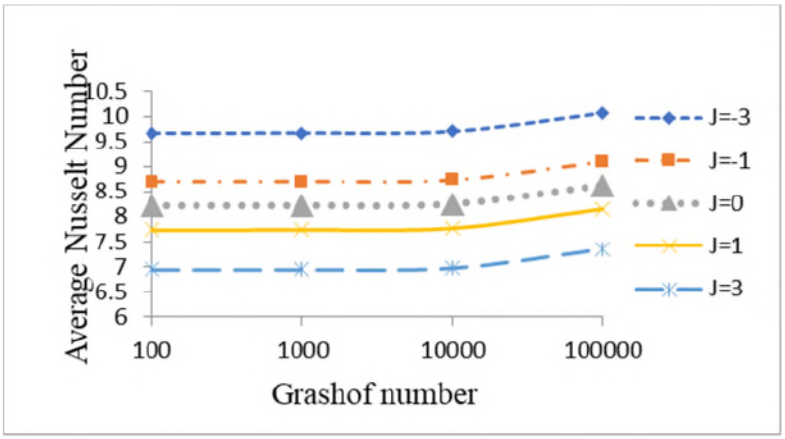

(c)

Figures 8 (a-c): Influence of *J* on Average Nusselt number for *Re*=1000, when *AR*= 1, 2, 3.

7. Conclusion

The analysis of steady laminar convective flow in a cavity driven by both shear and buoyancy forces has been performed. The cavity is filled with a fluid (*Pr=0.71*) that has both the ability to conduct electricity and also absorb or generate heat. A numerical solution that is anchored on the method of the finite element was generated. The implications of Grashof number, Reynolds number, adiabatic cylinder aspect ratio, heat generation/absorption parameter, magnetic field on fluid flow and heat transfer characteristics are summarized below.

1. It was discovered that for $Re = 100$ and the range of Grashof number ($10^2 \leq Gr \leq 10^5$) considered, adiabatic cylinder aspect ratio $AR = 2.0$ gave the highest heat transfer enhancement as further increase in aspect ratio beyond this critical value resulted in only an increase in material cost. However, when Re value was increased to 1000, the augmentation of heat transfer rises with improvement in aspect ratio. Hence for a low Reynold number flow regime, the adiabatic cylinder aspect ratio of 2.0 is recommended as the optimum.
2. For Grashof number, aspect ratio, and Reynolds number respectively in the ranges of ($10^2 \leq Gr \leq 10^5$), ($1.0 \leq AR \leq 2.0$), and ($100 \leq AR \leq 1000$), Hartmann number increment resulted in heat transfer suppression; and beyond $AR = 2.0$, the heat transfer rate for $Ha = 10$ approximates those transferred when the magnetic field was not considered.
3. For all the range of parameters considered, heat generation improvement declines heat transfer augmentation while heat transfer improvement is favored by the rising value of heat absorption.
4. The fluid flow and therrmal history are largely affected by the size of the adiabatic elliptical cylinder.
5. For low Reynolds number flow, the impact of cylinder size on heat transfer diminishes beyond $Gr=10^4$. But for high Reynolds (Re=1000), heat transfer augmentation is aided by increasing cylinder size.

References

[1] Abdulsahib A.D.,Al-Farhany K. (2021). Review of the Effects of Stationary/Rotating Cylinder in a Cavity on the Convection Heat Transfer in Porous Media with/without Nanofluid. Mathematical Modelling of Engineering Problems. 8(3): p. 356-364 10.18280/mmep.080304.

[2] Al-Chlaihawi K.K., Alaydamee H.H., Faisal A.E., Al-Farhany K.,Alomari M.A. (2021). Newtonian and non-Newtonian nanofluids with entropy generation in conjugate natural convection of hybrid nanofluid-porous enclosures: A review. Heat Transfer, 10.1002/htj.22372.

[3] Abdulkadhim A., Abed I.M.,Said N.M. (2021). An exhaustive review on natural convection within complex enclosures: Influence of various parameters. Chinese Journal of Physics. 74: p. 365-388 10.1016/j.cjph.2021.10.012.

[4] Abdulkadhim A., Abed I.M.,Mahjoub Said N. (2021). Review of Natural Convection Within Various Shapes of Enclosures. Arabian Journal for Science and Engineering. 46(12): p. 11543-11586 10.1007/s13369-021-05952-6.

[5] Redouane F., Jamshed W., Devi S.S.U., Amine B.M., Safdar R., Al-Farhany K., Eid M.R., Nisar K.S., Abdel-Aty A.H.,Yahia I.S. (2021). Influence of entropy on Brinkman–Forchheimer model of MHD hybrid nanofluid flowing in an enclosure containing rotating cylinder and undulating porous stratum. Scientific Reports. 11(1) 10.1038/s41598-021-03477-4.

[6] Al-Farhany K., Alomari M.A., Al-Saadi A., Chamkha A., Öztop H.F.,Al-Kouz W. (2022). MHD mixed convection of a Cu–water nanofluid flow through a channel with an open trapezoidal cavity and an elliptical obstacle. Heat Transfer. 51(2): p. 1691-1710 10.1002/htj.22370.

[7] Olayemi O.A., Al-Farhany K., Olaogun O., Ibiwoye M.O., Medupin R.O.,Jinadu A. (2021). Computational Fluid Dynamics Analysis of Mixed Convection Heat Transfer and Fluid Flow in a Lid-driven Square Cavity Subjected to Different Heating Conditions. IOP Conference Series: Materials Science and Engineering. 1107(1): p. 012201 10.1088/1757-899x/1107/1/012201.

[8] Khan M., Khan A.A.,Hasan M.N. *Numerical study of mixed convection heat transfer from a rotating cylinder inside a trapezoidal enclosure*. 2016. American Institute of Physics Inc. 10.1063/1.4958427.

[9] Yang L.,Farouk B. (1995). MIXED CONVECTION AROUND A HEATED ROTATING HORIZONTAL SQUARE CYLINDER IN A CIRCULAR ENCLOSURE. Numerical Heat Transfer, Part A: Applications. 28(1): p. 1-18 10.1080/10407789508913729.

[10] Chamkha A.J., Selimefendigil F.,Ismael M.A. (2016). Mixed convection in a partially layered porous cavity with an inner rotating cylinder. Numerical Heat Transfer, Part A: Applications. 69(6): p. 659-675 10.1080/10407782.2015.1081027.

[11] Olayemi O.A., Khaled A.F., Temitope O.J., Victor O.O., Odetunde C.B.,Adegun I.K. (2021). Parametric study of natural convection heat transfer from an inclined rectangular cylinder embedded in a square enclosure. Australian Journal of Mechanical Engineering, 10.1080/14484846.2021.1913853.

[12] Ismael M.A., Selimefendigil F.,Chamkha A.J. (2017). Mixed convection in a vertically layered fluid-porous medium enclosure with two inner rotating cylinders. Journal of Porous Media. 20(6): p. 491-511 10.1615/JPorMedia.v20.i6.20.

[13] Khajeh K., Jahanshaloo L., Ebrahimi S.,Aminfar H. (2018). Mixed convection heat transfer of Al2O3 nanofluid on the elliptical shapes: Numerical study of irreversibility. Journal of Applied Fluid Mechanics. 11(1): p. 177-189 10.29252/jafm.11.01.28080.

[14] Saieed A.N.A., Al-Mousawe S.T.M., Abtan A.A.,Habeeb L.J. (2020). Buoyancy Driven in An inclined CIrcular Enclosure with Elliptic Heat Source. Journal of Mechanical Engineering Research and Developments. 43(7): p. 62-74.

[15] Bhuiyan A.H.,Munshi M.J.H. (2018). Hydrodynamic Mixed Convection in a Lid- Driven Porous Square Cavity with Internal Heat Generating Elliptic Block. GANIT: Journal of Bangladesh Mathematical Society. 37(0): p. 175-183 10.3329/ganit.v37i0.35735.

[16] Alam M.S., Alim M.A.,Mollah M.S.H. *Mixed magnetoconvection in a lid-driven square enclosure with a sinusoidal vertical wall and joule heating*. 2017. Elsevier Ltd. 10.1016/j.proeng.2017.08.172.

[17] Chamkha A.J., Mansour M.A., Rashad A.M., Kargarsharifabad H.,Armaghani T. (2020). Magnetohydrodynamic mixed convection and entropy analysis of nanofluid in gamma-

shaped porous cavity. Journal of Thermophysics and Heat Transfer. 34(4): p. 836-847 10.2514/1.T5983.

[18] Mahfoud B., Benhacine H., Laouari A.,Bendjaghlouli A. (2020). Magnetohydrodynamic effect on flow structures between coaxial cylinders heated from below. Journal of Thermophysics and Heat Transfer. 34(2): p. 265-274 10.2514/1.T5805.

[19] Hu J. (2021). Motion of a neutrally buoyant elliptical particle in a lid-driven square cavity. European Journal of Mechanics, B/Fluids. 85: p. 124-133 10.1016/j.euromechflu.2020.09.008.

[20] Chamkha A.J. (2002). HYDROMAGNETIC COMBINED CONVECTION FLOW IN A VERTICAL LID-DRIVEN CAVITY WITH INTERNAL HEAT GENERATION OR ABSORPTION. Numerical Heat Transfer, Part A: Applications. 41(5): p. 529-546 10.1080/104077802753570356.

[21] Rahman M.M., Öztop H.F., Rahim N.A., Saidur R.,Al-Salem K. (2011). MHD Mixed Convection with Joule Heating Effect in a Lid-Driven Cavity with a Heated Semi-Circular Source Using the Finite Element Technique. Numerical Heat Transfer, Part A: Applications. 60(6): p. 543-560 10.1080/10407782.2011.609087.

[22] Mondal M.K., Biswas N., Sarkar U.K., Manna N.K.,Mandal D.K. (2021). Effect of partial wall motion on MHD mixed convection heat transfer undergoing in a porous cavity filled with Cu–water nanofluid with a centrally mounted heat source. IOP Conference Series: Materials Science and Engineering. 1080(1): p. 012025 10.1088/1757-899x/1080/1/012025.

[23] Alam M.S., Mollah M.S.H., Alim M.A., Ali M.M.,Munshi M.J.H. *Effect of Rayleigh number magneto-convection in a lid-driven square cavity with a sinusoidal wall*. 2019. American Institute of Physics Inc. 10.1063/1.5115866.

[24] Rajarathinam M., Nithyadevi N.,Chamkha A.J. (2018). Heat transfer enhancement of mixed convection in an inclined porous cavity using Cu-water nanofluid. Advanced Powder Technology. 29(3): p. 590-605 10.1016/j.apt.2017.11.032.

[25] Nosonov I.I.,Sheremet M.A. (2018). Conjugate mixed convection in a rectangular cavity with a local heater. International Journal of Mechanical Sciences. 136: p. 243-251 10.1016/j.ijmecsci.2017.12.049.

[26] El Moutaouakil L., Zrikem Z.,Abdelbaki A. (2017). Lattice Boltzmann Simulation of Natural Convection in an Annulus between a Hexagonal Cylinder and a Square Enclosure. Mathematical Problems in Engineering. 2017 10.1155/2017/3834170.

[27] Soomro F.A., Haq R.U., Algehyne E.A.,Tlili I. (2020). Thermal performance due to magnetohydrodynamics mixed convection flow in a triangular cavity with circular obstacle. Journal of Energy Storage. 31 10.1016/j.est.2020.101702.

[28] Taamneh Y.,Bataineh K. (2017). Mixed convection heat transfer in a square lid-driven cavity filled with Al2O3-Water Nanofluid. Strojniski Vestnik/Journal of Mechanical Engineering. 63(6): p. 383-393 10.5545/sv-jme.2017.4449.

[29] Xiong P.Y., Hamid A., Iqbal K., Irfan M.,Khan M. (2021). Numerical simulation of mixed convection flow and heat transfer in the lid-driven triangular cavity with different obstacle configurations. International Communications in Heat and Mass Transfer. 123 10.1016/j.icheatmasstransfer.2021.105202.

[30] Al-Farhany K.,Abdulsahib A.D. (2021). Study of mixed convection in two layers of saturated porous medium and nanofluid with rotating circular cylinder. Progress in Nuclear Energy. 135 10.1016/j.pnucene.2021.103723.

[31] Abdulsahib A.D.,Al-Farhany K. *Numerical Investigation of the nanofluid mixed convection on two layers enclosure with rotating cylinder: High Darcy Number Effects*. 2020. IOP Publishing Ltd. 10.1088/1757-899X/928/2/022001.

[32] Deb D., Poudel S.,Chakrabarti A. (2017). Numerical Simulation of Hydromagnetic Convection in a Lid-driven Cavity Containing a Heat Conducting Elliptical Obstacle with Joule Heating. International Journal of Engineering Research and. V6 10.17577/IJERTV6IS080055.

[33] Adekeye T., Adegun I.K., Okekunle P.O., Hussein A.K., Oyedepo S.O., Adetiba E.,Fayomi O.S.I. (2017). Numerical Analysis of the Effects of Selected Geometrical Parameters and Fluid Properties on MHD Natural Convection Flow in an Inclined Elliptic Porous Enclosure with Localized Heating. Heat Transfer - Asian Research. 46(3): p. 261-293 10.1002/htj.21211.

[34] Toghraie D.,Shirani E. (2020). Numerical simulation of water/alumina nanofluid mixed convection in square lid-driven cavity: Effect of magnetic field using a two-phase model.

International Journal of Numerical Methods for Heat and Fluid Flow. 30(5): p. 2781-2807 10.1108/HFF-02-2019-0114.

[35] Das D., Roy M.,Basak T. (2017). Studies on natural convection within enclosures of various (non-square) shapes – A review. International Journal of Heat and Mass Transfer. 106: p. 356-406 https://doi.org/10.1016/j.ijheatmasstransfer.2016.08.034.

[36] Padhi P., Udhayakumar S., Sekhar T.V.S.,Sivakumar R. (2021). Thermo-magneto-convection and mechanism of multiple eddy formation due to applied magnetic field in a lid-driven cavity. Engineering Research Express. 3(1) 10.1088/2631-8695/abde4d.

[37] Alomari M.A., Al-Farhany K., Hashem A.L., Al-Dawody M.F., Redouane F.,Olayemi O.A. (2021). Numerical study of mhd natural convection in trapezoidal enclosure filled with (50%mgo-50%ag/water) hybrid nanofluid: Heated sinusoidal from below. International Journal of Heat and Technology. 39(4): p. 1271-1279 10.18280/ijht.390425.

[38] Venkatadri K., Gouse Mohiddin S.,Suryanarayana Reddy M., Numerical Analysis of Unsteady MHD Mixed Convection Flow in a Lid-Driven Square Cavity with Central Heating on Left Vertical Wall, J. Prakash, et al., Editors. 2018, Springer Heidelberg. p. 355-370.

[39] Selimefendigil F., Ismael M.A.,Chamkha A.J. (2017). Mixed convection in superposed nanofluid and porous layers in square enclosure with inner rotating cylinder. International Journal of Mechanical Sciences. 124-125: p. 95-108 10.1016/j.ijmecsci.2017.03.007.

[40] Zainab K.R. (2013). Study Natural Convection in a Porous Trapezoidal Cavity with a Square Body at the Center of the Enclosure. Engineering and Technology Journal. 31(14 Part (A) Engineering): p. 2632-2649.

[41] Al-Farhany K., Al-Chlaihawi K.K., Al-dawody M.F., Biswas N.,Chamkha A.J. (2021). Effects of fins on magnetohydrodynamic conjugate natural convection in a nanofluid-saturated porous inclined enclosure. International Communications in Heat and Mass Transfer. 126 10.1016/j.icheatmasstransfer.2021.105413.

[42] Al-Farhany K., Al-dawody M.F., Hamzah D.A., Al-Kouz W.,Said Z. (2021). Numerical investigation of natural convection on Al2O3–water porous enclosure partially heated with two fins attached to its hot wall: under the MHD effects. Applied Nanoscience (Switzerland), 10.1007/s13204-021-01855-y.

[43] Khanafer K.M.,Chamkha A.J. (1999). Mixed convection flow in a lid-driven enclosure filled with a fluid-saturated porous medium. International Journal of Heat and Mass Transfer. 42(13): p. 2465-2481 10.1016/S0017-9310(98)00227-0.

[44] Iwatsu R., Hyun J.M.,Kuwahara K. (1993). Mixed convection in a driven cavity with a stable vertical temperature gradient. International Journal of Heat and Mass Transfer. 36(6): p. 1601-1608 10.1016/S0017-9310(05)80069-9.

[45] Ali M.M., Akhter R.,Alim M.A. (2022). Magneto-mixed convection in a lid driven partially heated cavity equipped with nanofluid and rotating flat plate. Alexandria Engineering Journal. 61(1): p. 257-278 10.1016/j.aej.2021.05.003.

Magnetoconvection around an elliptic cylinder placed in a lid-driven square enclosure subjected to internal heat generation or absorption

Olayemi, Olalekan Adebayo

2022-04-01

Olayemi OA, Al-Farhany K, Obalalu AM, et al., (2022) Magnetoconvection around an elliptic cylinder placed in a lid-driven square enclosure subjected to internal heat generation or absorption. Heat Transfer, Volume 51, Issue 6, September 2022, pp. 4950-4976

https://doi.org/10.1002/htj.22530